VORTEX SYSTEMS AND THE INTERACTION BETWEEN AN AIR INLET AND THE GROUND

Arne Karlsson , Laszlo Fuchs
Dep. of Mechanics and Dep. of Aeronautics, KTH, Stockholm, Sweden
Div. of Fluid Mechanics, LTH, Lund, Sweden

Keywords: *CFD, LES, air inlet, inlet vortex system*

Abstract

The flow in the neighbourhood of and into an inlet to a gas turbine engine close to the ground is studied through Large Eddy Simulations (LES). When air is sucked into the air inlet a vortex system develops between the air inlet and the ground. The flow influenced by this vortex system is not only turbulent but also contains larger unsteady vortex structures. These larger vortex structures are characterized by their shape and their frequencies. From the frequencies it is shown that there are several modes in the dynamics of these vortex structures following upon each other. The duration of each of these modes can vary and the character of the flow can be either clearly turbulent or become partially laminar and transitional. This behaviour is qualitatively compared to and verified by experimental data found in the literature. Results indicating that part of the dynamics of the vortex system can survive a mode transition is presented. It is also shown that a velocity gradient far upstream with vertical vorticity lines will have influence on the vortex system.

1 Introduction

If the air inlet of a gas turbine engine is located close to the ground it works like a big vacuum cleaner and foreign objects can be ingested into it. However, the low pressure created by the compressor is not enough to lift debris from the ground. Earlier experimental work shows that a vortex, or rather a vortex system, between the ground and the air inlet can develop. It is the suction created at the foot point of a vortex between the ground and the air inlet that can lift objects from the ground and give these objects such high impulse that they are sent upwards and can reach the height of the air inlet. This vortex will be called the *inlet vortex*.

Investigations into this problem started during the early 50ties and identified the vortex between the ground and the air inlet as the primary source for foreign object ingestion into the air inlet. One of these early works is by Rodert & Garret [17] (RG). With the advent, towards the end of the 60ties, of high by-pass-ratio engines placed in nacelles under the wings of low-winged airliners there were a revival of interest for the inlet vortex problem. One work from this period is by Glenny & Pyestock [7] (GP).

Both RG and GP showed by experiments that particles can be lifted from the ground by the inlet vortex. In the work by GP there are also given quantitative criteria on different parameters for when the inlet vortex is strong enough to lift objects from the ground. In both the works by RG and GP it is noticed that the foot point on the ground of the inlet vortex is not stationary but is moving around.

During the period up to the mid 70ties several, mainly experimental, works were published all aiming towards identifying the underlying phenomena and then trying to find technical solutions to avoid getting debris sucked into the air inlet. Some examples are the works by Colehour

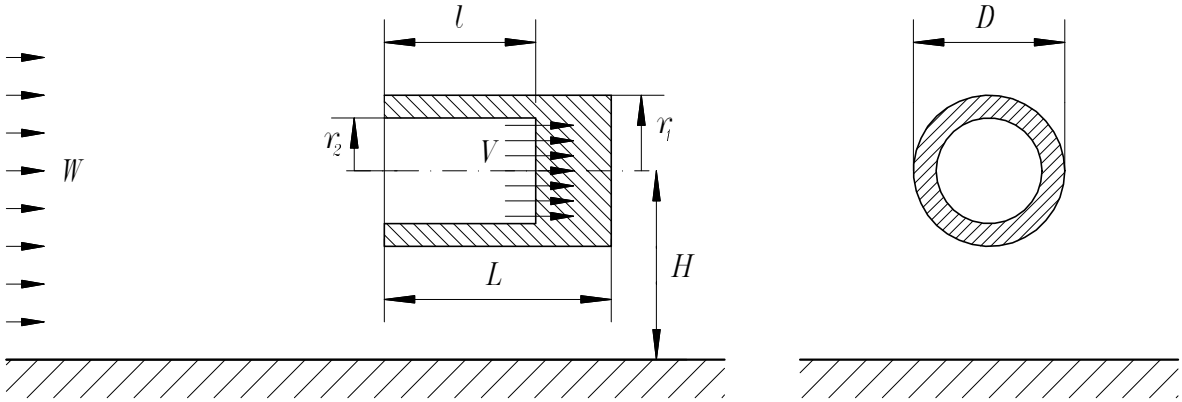

Fig. 1 The model problem for the air inlet.

& Farquhar [4], Motycka, Walter & Muller [13] and Motycka & Walter [12].

A first step towards a deeper understanding of the problem was taken by Bissinger & Braun [2]. In a water tunnel investigation they note that there is not only an inlet vortex but a whole vortex system. They also note that this vortex system is unsteady in nature and that it can break up and regenerate.

A group at MIT later continued the investigations towards a deeper physical understanding of the inlet vortex problem (de Siervi, Viguier, Greitzer & Tan [5], Liu, Greitzer & Tan [11], Shin, Cheng, Greitzer & Tan [18] and Shin, Greitzer, Cheng, Tan & Shippee [19]). One conclusion from this group is to confirm results from others that an inlet vortex can develop when vertical vorticity lines are sucked into the air inlet and amplified by both superposition and stretching. The MIT group also identifies another mechanism that can give rise to an inlet vortex. If the centre line of the air inlet is not aligned with the ambient wind an inlet vortex can develop without any ambient vorticity.

The inlet vortex problem has recently been revisited in two papers by Nakayama & Jones [14, 15] (NJ). They present experimental results on an inlet close to a simulated fuselage. They also perform numerical simulations based on a potential flow model as well as an empirical study to find criteria for the formation of an inlet vortex. The latter part of that study is based mainly on data published by other researchers. The numerical predictions presented by NJ differs by about a factor 2 from the empirical criterion.

A work on a similar problem has recently been published by Behrouzi & McGuirk [1]. They study the interaction between two vertical jets impinging a ground plane on both sides of an air inlet with horizontal axis. Their numerical simulations are based on the Reynolds Averaged Navier-Stokes (RANS) equations and the k-ε turbulence model. They also compare with experiments presented in another paper and conclude that there are errors also in their steady state time-averaged predictions. They suggest moving to either a Reynolds stress transport turbulence model or an LES-based approach.

The present work is one part of a larger study aiming to be a contribution to the physical understanding of the inlet vortex problem with emphasis on unsteady and/or oscillatory phenomena. This study is carried out through numerical simulations of a model problem as defined below. Contrary to previous theoretical works, which are mainly based on steady state potential flow models, the present analysis is based on the time-dependent Navier-Stokes equations. All the larger scales in the problem are resolved by adequate temporal and spatial resolution and we perform a Large Eddy Simulation (LES). Several interesting phenomena are revealed. One is the presence of different modes (vortex structures and frequencies) as shown in a previous paper

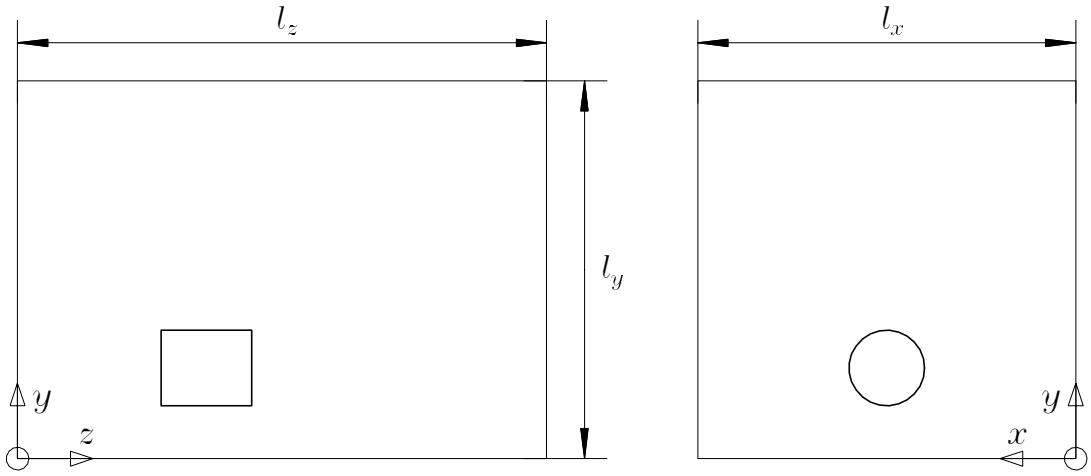

Fig. 2 The computational domain with the air inlet.

(Karlsson & Fuchs [10]). One main topic of this paper is a closer study of the dynamics of these modes. We also consider the influence of vertical vorticity lines along the inflow boundary to our computational domain.

2 Model problem

Consider a jet engine close to the ground. This problem is modelled as sketched in Figure 1. The engine is either moving slowly with speed W relative the ground or is fixed but placed in a head wind with the same speed.

The air inlet is modelled by a cylinder with circular cross section and diameter $D = 2r_1$. The air inlet centre line is parallel to the ground and placed at height H above it. The height H is of the same order of magnitude as the diameter D. The inner radius of the air inlet is r_2, its overall length is L and there is an open part inside it with depth l.

Air is sucked into the air inlet by prescribing a normal velocity V at the inner vertical (downstream) face of the air inlet as shown in Figure 1. On the side and top boundaries undisturbed boundary conditions are set and on the outflow boundary we set vanishing gradients and enforce global conservation of mass.

3 Governing equations

The flow in the model problem presented above is solved with the time-dependent incompressible Navier-Stokes equations. These equations are written in non-dimensional form with the outer diameter D of the model air inlet as characteristic length and the suction velocity V as characteristic speed. The Reynolds number is defined as $Re = DV/\nu$ where ν is the kinematic viscosity of the air.

Using the Cartesian tensor notation and the summation convention the governing equations are

$$\frac{\partial u_i}{\partial x_i} = 0 \tag{1}$$

$$\frac{\partial u_i}{\partial t} + \frac{\partial \left(u_j u_i\right)}{\partial x_j} = -\frac{\partial p}{\partial x_i} + \frac{1}{Re}\frac{\partial^2 u_i}{\partial x_j \partial x_j} \tag{2}$$

These equations are filtered through a spatial filter $G(\vec{x})$. The filtered variables are defined by

$$\overline{f}\left(\vec{x},t\right) = \int f\left(\vec{x}',t\right) G\left(\vec{x}-\vec{x}'\right) d\vec{x}' \tag{3}$$

Here the filter function G is assumed to be commutative, associative and distributive with respect to differentiation. After applying such a filter on the equations (1) and (2) the following equations are obtained

$$\frac{\partial \overline{u}_i}{\partial x_i} = 0 \tag{4}$$

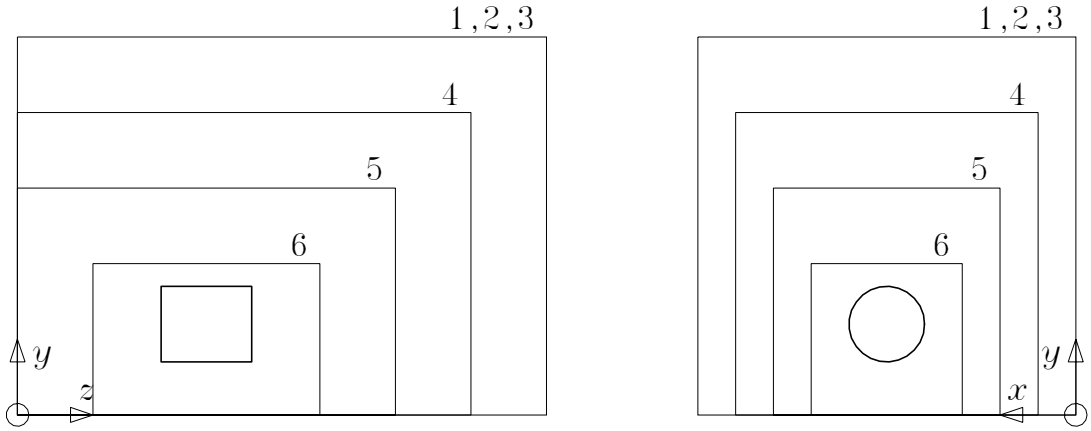

Fig. 3 Extension of the meshes on different MGM levels.

$$\frac{\partial \overline{u}_i}{\partial t} + \frac{\partial \left(\overline{u_i u_j}\right)}{\partial x_j} = -\frac{\partial \overline{p}}{\partial x_i} + \frac{1}{Re}\frac{\partial^2 \overline{u}_i}{\partial x_j \partial x_j} \quad (5)$$

If the sub-grid scale (SGS) turbulent stress is defined as

$$\tau_{ij} = \overline{u_i u_j} - \overline{u}_i \overline{u}_j \quad (6)$$

the filtered momentum equations become

$$\frac{\partial \overline{u}_i}{\partial t} + \frac{\partial \left(\overline{u}_i \overline{u}_j\right)}{\partial x_j} = -\frac{\partial \overline{p}}{\partial x_i} + \frac{1}{Re}\frac{\partial^2 \overline{u}_i}{\partial x_j \partial x_j} - \frac{\partial \tau_{ij}}{\partial x_j} \quad (7)$$

The SGS stress term must be modelled in terms of the filtered variables. However, in this case we are only interested in studying spatial and temporal scales that are large compared to the spatial and temporal finite difference resolutions. In such cases it is argued [3, 8, 10] that the last term is, at least in terms of dissipation, accounted for through the discretization process. From this point of view the only requirement on the SGS stress model is that it has enough dissipation so that there is no build-up of small scale turbulent kinetic energy. We do not include any explicit SGS stress model and this can be motivated from our solutions where we estimate that as much as 99% of the total turbulent kinetic energy is resolved.

4 Mathematical and computational model

The computational domain is shown in Figure 2. The centre line of the air inlet is aligned with the z-axis and the computational domain has the dimensions (l_x,l_y,l_z) as shown in the figure. The dimension of the air inlet is chosen so that $D = L = 1$ and for the computational domain (l_x,l_y,l_z) = (5,5,7). The air inlet is placed inside the computational domain so that its centre is located at (x,y,z) = (2.5,H,2.5). In the main part of the computations reported here $H = 1$.

The ground plane is stationary and at $y = 0$ and here the no-slip boundary condition is applied. Note that this implies that the air inlet is stationary relative the ground and is placed in a head wind W as shown in Figure 1. In addition to the boundary conditions on the velocity vector given in Section 2 a random disturbance is applied on the inflow boundary velocity W. If nothing else is stated the amplitude of this disturbance is 5% of W. Also a linear velocity gradient of W in the spanwise (x-) direction can be applied. Such a velocity gradient yields a vorticity component in the direction normal to the ground. In such a case the figures given below for W applies at the mid plane ($x = l_x/2$).

The Navier-Stokes equations are discretized in the computational domain using a staggered Cartesian grid with uniform grid spacings. Time marching is performed with a fully implicit method and in space a fourth order finite-difference discretization is used. The discrete equations are solved using a Multi-Grid Method (MGM) and local mesh refinements. The solu-

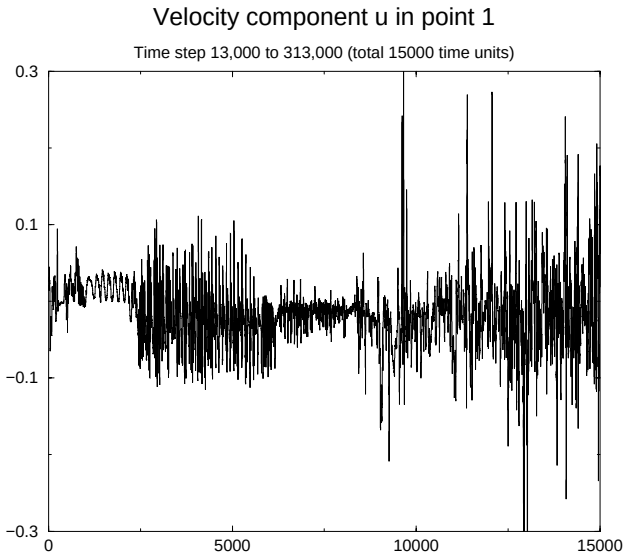

Fig. 4 Time evolution of the velocity component u in one point of the flow field showing several different modes.

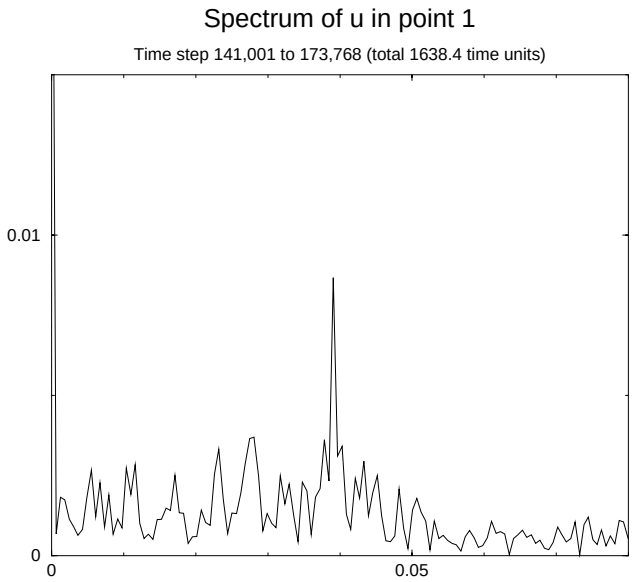

Fig. 5 Low frequency part of the spectrum of the velocity component u in Point 1 in the time interval from t = 6 400 to 8 038.4 time units (Mode 3).

tion algorithm as well as an analysis of its accuracy have been given by Fuchs [6] and by Olsson & Fuchs [16].

The high order spatial discretization is of prime importance in this case. Preliminary test with second order spatial discretization failed to generate the time-dependence in the solution that was observed experimentally. With second order spatial discretization the solution converged to a steady state.

In the MGM solver we use 6 levels. The 3 coarsest grids cover the full computational domain. Each new mesh is obtained by halving the grid size of the previous grid. The grid size is $h_x = h_y = h_z = 1/32$ on the finest local grid (level 6) and this local grid has the following extent: $1.5 \leq x \leq 3.5$, $0 \leq y \leq 2$ and $1 \leq z \leq 4$, respectively. The extent of the other grids are shown in Figure 3. Altogether there are over 700 000 grid points in the computational domain.

5 Results

The model problem described in Section 2 has been solved for the following parameter values

$$L = D = 1 \quad , \quad \frac{H}{D} = 1 \quad ,$$

St	t_p	$I_u \cdot 10^3$	$I_v \cdot 10^3$	$I_w \cdot 10^3$
0.001831	546.1	–	0.6	–
0.003052	327.7	–	0.4	–
0.005493	182.0	2.7	0.7	4.2
0.006714	148.9	2.3	–	2.5
0.007934	126.0	1.9	(0.7)	5.6
0.009155	109.2	(1.1)	(0.8)	8.6
0.010986	91.0	–	(0.6)	11.2
0.028076	35.6	3.7	(1.2)	–
0.037842	26.4	3.6	1.3	–
0.039062	25.6	8.7	2.3	(2.2)
0.040283	24.8	(3.4)	1.2	(1.6)

Table 1 The three lowest frequencies in the spectra of the velocity components at Point 1 in the time interval from t = 6 400 to 8 038.4 time units (Mode 3). St is the non-dimensional frequency or Strouhal number, $t_p = 1/St$ is the period time and I is the amplitude of that Fourier component. This table also includes the three most intense frequencies in each velocity component. Also included in parenthesis are the amplitudes of the other velocity components, if such frequencies exists.

$$l = 0.55 \quad , \quad r_2 = 0.42 \quad , \quad W = 0.1 \quad ,$$
$$V = 1 \quad , \quad Re = \frac{VD}{\nu} = 50\,000 \qquad (8)$$

The time integration is performed with a time step $h_t = 0.05$ time units ($= D/V$).

The time evolution is followed by monitoring the solution in some points in each time step. Figure 4 shows the time evolution of the velocity component u in the x-direction in one of these points (called Point 1 which is located at (x,y,z) = (2.8,0.03125,1.75)). This velocity component is followed from time step 13 000 to time step 313 000 and time $t = 0$ is in this case arbitrarily set at time step 13 000.

Initially there is a transient behaviour of the solution. At about t = 1 000 the flow enters a mode with relatively low frequency oscillations. The solution stays in this mode for about 1 000 time units and then it enters a transitional phase lasting for about 400 to 500 time units. Thereafter a new mode is reached with relatively high frequency oscillations. The solution is in this mode for about 3 000 time units. As seen in Figure 4 this mode is followed by a third and a fourth mode. Between each mode there is a transition of phase lasting for about 500 time units.

The first two modes have been discussed in a previous paper ([10]). This analysis is not repeated here but the results will be used in a comparison between the behaviour of the solution in all four modes.

The third mode is studied by calculating the spectra of the velocity components for a time interval from t = 6 400 to 8 038.4 time units (totally 1 638.4 time units or 32 768 time steps). The low frequency part of the spectrum is shown in Figure 5 for the same velocity component and location as in Figure 4. The most energetic frequency is found for the Strouhal number (frequency normalized with V/D) St = 0.03906 corresponding to a period time $t_p = 1/St$ = 25.6 time units. As seen from Table 1 this is also the most energetic frequency in the v-component while the most energetic frequency in the w-component is found for St = 0.01099 or t_p = 91.0 time units. (In Table 1 the lowest frequency found in the spectrum of the u-component has been excluded due to a too narrow support in the studied time interval. It is also seen from Figure 5 that, from the same reason, the low end of the spectrum is not fully resolved.)

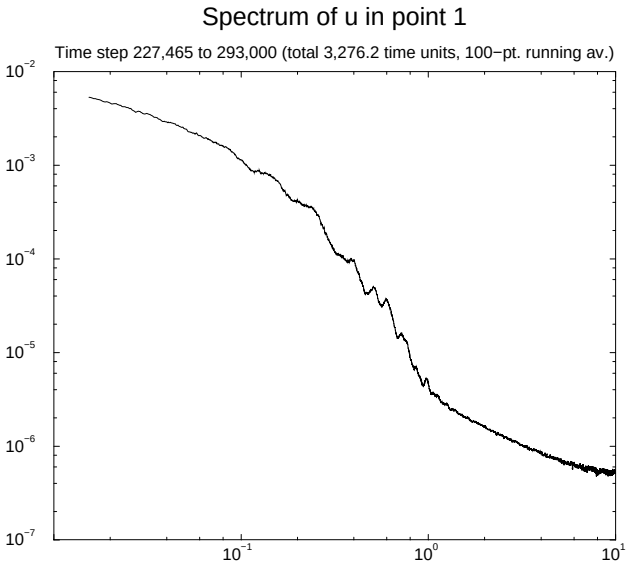

Fig. 6 High frequency part of the spectrum of the velocity component u in Point 1 in the time interval from t = 10 723.2 to 14 000 time units (Mode 4).

The high frequency end of the third mode spectra indicates no presence of any significant turbulence in the flow (these spectra are not shown here).

The fourth mode velocity component spectra is calculated in the time interval from t = 10 723.2 to 14 000 time units (totally 3 276.8 time units or 65 536 time steps). The high frequency part of this spectrum is shown in Figure 6 and the low frequency part in Figure 7 for u at Point 1.

In the high frequency part of the spectrum shown in Figure 6 it is seen that significant amount of turbulence is present in the flow. This spectrum also reveals a resolved range of about one order of magnitude which lies in the inertial subrange. The change in slope at about $St = 10^0$ marks the resolution limit of the simulations. From the corresponding spectrum for the turbulent kinetic energy k we deduce that over 99% of the turbulent kinetic energy is resolved.

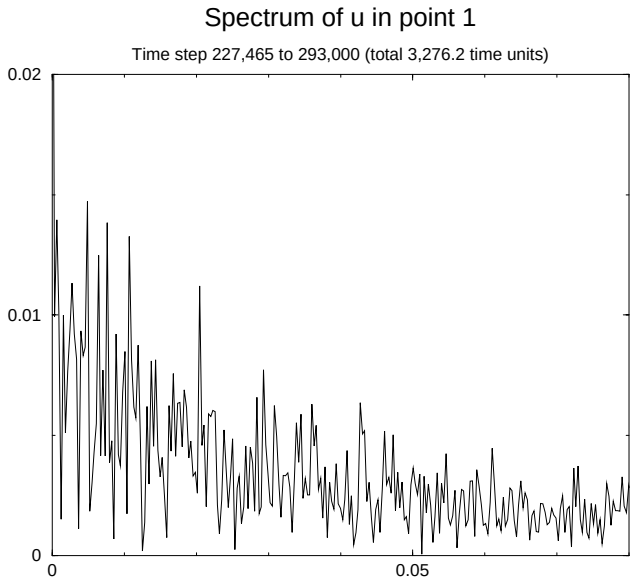

Fig. 7 Low frequency part of the spectrum of the velocity component u in Point 1 in the time interval from t = 10 723.2 to 14 000 time units (Mode 4).

St	t_p	$I_u \cdot 10^3$	$I_v \cdot 10^3$	$I_w \cdot 10^3$
0.000916	1092.3	–	1.6	–
0.001221	819.2	–	–	6.8
0.001526	655.4	10.0	2.5	–
0.002136	468.1	–	–	5.3
0.002441	409.6	–	1.8	–
0.002746	364.1	11.3	–	6.0
0.003967	252.1	9.3	3.0	–
0.004883	204.8	14.7	–	13.6
0.007629	131.1	13.8	–	(7.0)
0.010071	99.3	(8.5)	–	12.8
0.010681	93.6	13.3	–	–
0.011597	86.2	–	–	10.8
0.026856	37.2	(4.6)	2.5	–
0.031128	32.1	–	2.9	–

Table 2 The three lowest frequencies in the spectra of the velocity components in Point 1 in the time interval from t = 10 723.2 to 14 000 time units (Mode 4). Further details are given in the caption to Table 1.

This spectrum for the turbulent kinetic energy in Point 1 during Mode 2 is presented in [10].

Comparing the low frequency part of the spectra shown in Figure 5 and Figure 7 reveals a big difference. During Mode 4 there are many modes in contrast to Mode 3. One can also see that, at least for the velocity component u, the most energetic frequencies are found at the low end of this spectrum. From Table 2 it is seen that the two most energetic frequencies are found for Strouhal numbers St = 0.00488 and 0.00763, respectively, corresponding to the period times t_p = 204.8 and 131.1 time units, respectively. The spectrum for the w-component has the same appearance while for the v-component the low end of the spectrum is more spread out (these two spectra are not shown here). One can also note from Table 2 that the most energetic frequency in both the u- and the w-component is found for St = 0.00488.

Now comparing the spectra for all four modes some observations can be made. First it is noted that the solution is in a distinct mode for a period of time depending on the particular mode. This distinct mode of motion will be broken up and, after a transition period, it will be replaced by another distinct mode with different dynamics. This behaviour has been observed previously in the experiments by Bissinger & Braun [2] (BB). They points out that: “A vortex would be formed and would break down without any change in the test parameters, its pieces floating downstream. Seconds later it would start forming again.” Comparing dimensional parameters between the experiments by BB and the computations presented here shows that 1 second in the experiments corresponds to about 100 time units in our computations. Hence, the mode transition reported in the experiments can be observed in our computations.

From the high-frequency part of the spectra of all four modes it can be noted that there is no presence of any significant turbulence in the flow for Modes 1 and 3 while the spectra for Modes 2 and 4 show that a significant amount of turbulence is present in the flow. Hence, the shift between different modes can also have an influence on (or is influenced by) the turbulence level in the

flow.

The difference in turbulence level can also be seen in the low-frequency part of the spectra where the spectra for Modes 2 and 4 have a similar appearance with a large number of frequency components. Modes 1 and 3 contain a few well defined frequencies.

The most energetic frequencies in the different modes are for the u-component at Point 1: St = 0.00610 in Mode 1, St = 0.01129 in Mode 2, St = 0.03906 in Mode 3 and St = 0.00488 in Mode 4. As seen from this no specific pattern can be detected. Looking instead on the lowest frequencies one obtains: St = 0.00610, 0.00916, 0.00549 and 0.00092 for the four modes, respectively. No clear pattern can be detected here either. This seems to indicate that when one mode is replaced by the next one the dynamics of the complete flow is changed.

However, some common pattern can be found. The second lowest frequency in the u-component at Point 1 is St = 0.00977 during Mode 1 and this frequency cannot be found in the v- and w-components. But, this frequency pops up as the second lowest frequency in the v-component and as the lowest frequency in the w-component during Mode 2. During Modes 3 and 4 this frequency is not found in any velocity component at Point 1 but in the v-component at Point 2 during Mode 4. (Point 2 is located at (x,y,z) = (2.35,0.03125,1.75). Detailed data for this point is neither presented here nor in [10].)

Further, the lowest frequency in the u- and v-component at Point 1 is St = 0.00916 during Mode 2. This frequency is also found in all three velocity components in Point 1 during Mode 3 (as well as in all three velocity components in Point 2). During Mode 4 this frequency is found in the v- and w-components at Point 1 and in the v-component at Point 2.

Hence, it seems that at least some of the dynamics in the flow survives a mode shift but can move to another part of the flow field and/or to another velocity component. At the same time it can be a large change in the energy content of that frequency. To deepen the understanding further of what is going on in the flow field a more detailed study is required.

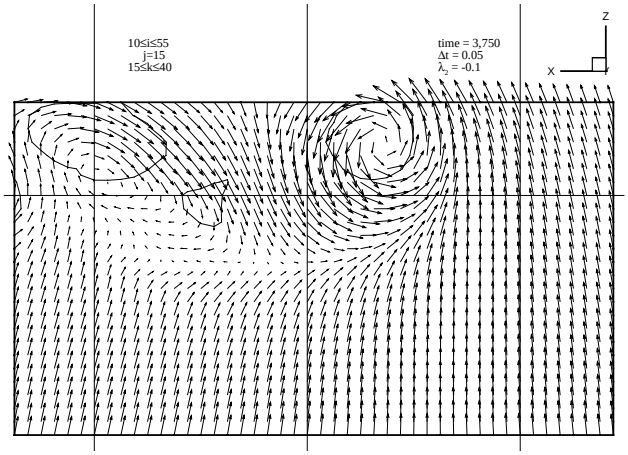

Fig. 8 Velocity vectors and iso-λ_2 lines in a horizontal plane at y = 14/32 and for $57/32 < x < 102/32$ and $46/32 < z < 71/32$ in a computation with $H = 1.25$ and after 75 000 time steps. Here $\lambda_2 = -0.1$.

The influence of the height H (see Figure 1) between the air inlet and the ground as well as from vertical vorticity lines at the inflow boundary have been studied. First the height H is increased from 1 to 1.25 while all other parameters are kept unchanged. The computation is restarted with this geometry and run for 75 000 time steps (3 750 time units). From a time history similar to the one shown in Figure 4 it is seen that initial transients disappear and that the solution has passed through a first transition of mode (this time history is not shown in this paper). At this point the velocity gradient $\partial W/\partial x$ = 0.01 is introduced at the inflow boundary. The simulations are run for further 15 000 time steps. In parallel the original simulation is continued for yet another 15 000 time steps so that both these cases are run for total 4 500 time units.

Figure 8 depicts the velocity vectors in a horizontal plane between the air inlet and the ground. In the figure iso-lines for the eigenvalue λ_2 to the tensor $S_{il}S_{lj} + \Omega_{il}\Omega_{lj}$, where S_{ij} and Ω_{ij} are the symmetric and antisymmetric part of the velocity gradient tensor $\partial u_i/\partial x_j$, respectively, also is included. A vortex is defined by an iso-surface for which the intermediate (λ_2) eigenvalue vanishes.

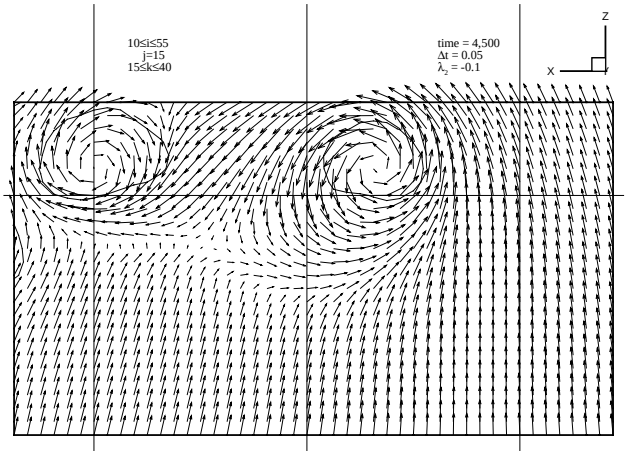

Fig. 9 Velocity vectors and iso-λ_2 lines after 90 000 time steps. Other data as in the caption to figure 8.

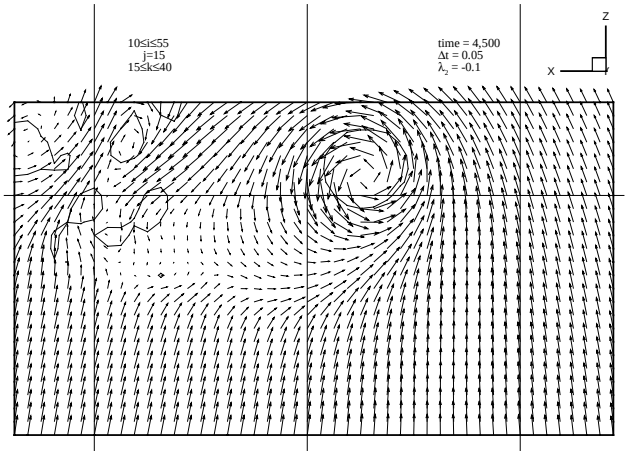

Fig. 10 Velocity vectors and iso-λ_2 lines after 90 000 time steps. After 75 000 time steps a velocity gradient has been introduced on the inflow boundary. See the text for details. Other data as in the caption to figure 8.

The λ_2-method described by Jeong & Hussain [9] is used to identify vortex structures. In Figure 8 a relatively strong and almost vertical vortex can be seen close to the vertical symmetry plane under the inlet. Another (weaker and oblique) vortex is also seen to the left in the figure.

After further 15 000 time steps this second vortex has been strengthen as seen in Figure 9. At the same time the first vortex has moved upstream and slightly towards the symmetry plane.

This picture can be compared with the one shown in Figure 10 obtained after 75 000 time steps with a velocity gradient. The computation is then continued for another 15 000 time steps so that, in all, 90 000 time steps are made. In this case the main vortex is found slightly more upstream and closer to the symmetry plane than in the case shown in Figure 9. The second vortex to the left has disappeared. In this horizontal plane this vortex seems to have been broken up into small pieces. However, this vortex is still found further up and closer to the air inlet (not shown here).

The results clearly show that vertical vorticity lines at the inflow boundary have an influence on the structure of the inlet vortex system. However, the results shown in these figures are a little surprising. A positive velocity gradient $\partial W/\partial x$ on the inflow boundary generates clockwise vorticity in an *xz*-plane. One would expect clockwise vortices to be amplified and counterclockwise to be damped. Here the result seems to be the opposite. Preliminary computations, with lower order spatial discretization, have shown exactly the expected behaviour although this spatial discretization only gives rise to a steady state solution. The mechanism by which the upstream vorticity interacts with the air inlet vortex system has to be studied further.

6 Discussion and concluding remarks

Our Large Eddy Simulations show a very rich and unsteady behaviour of the vortex system close to an air inlet in the proximity of the ground. It has been shown that the dissipation introduced by the discretization of the governing equations is enough to study the dynamics of the large scale structures of this turbulent flow field.

Several phenomena that have been observed experiments could be confirmed through LES. One is the transition between different modes of motion of the vortex system. We characterize the different modes by analyzing the Fourier content of the velocity vector at some monitoring stations.

The structure of the vortex system has been studied by analyzing the eigenvalues of a tensor computed from the velocity gradient tensor. The dynamics of the vortex system (not shown) sheds some light on the physics of the air-inlet vortex system.

Another phenomenon is the influence from upstream vertical vorticity on this system as shown experimentally by Siervi et. al. [5]. However, this influence must be analysed further, mainly by a continuation of the simulation.

References

[1] Behrouzi P and McGuirk J. Computational fluid dynamics prediction of intake ingestion relevant to short take-off and vertical landing aircraft. *Proceedings of The Institution of Mechanical Engineers, Part G – Journal of Aerospace Engineering*, Vol. 213, pp 131–142, 1999.

[2] Bissinger N. C and Braun G. W. On the inlet vortex system. NASA CR 132536, 1974.

[3] Boris J. P, Grinstein F. F, Oran E. S, and Kolbe R. L. New insight into large eddy simulation. *Fluid Dynamics Research*, Vol. 10, pp 199–228, 1992.

[4] Colehour J. L and Farquhar B. W. Inlet vortex. *Journal of Aircraft*, Vol. 8, No 1, pp 39–43, 1971.

[5] de Siervi F, Viguier H. C, Greitzer E. M, and Tan C. S. Mechanisms of inlet-vortex formation. *Journal of Fluid Mechanics*, Vol. 124, pp 173–207, 1982.

[6] Fuchs L. A local mesh refinement technique for incompressible flows. *Computers & Fluids*, Vol. 14, pp 69–81, 1986.

[7] Glenny D. E and Pyestock N. G. T. E. Ingestion of debris into intakes by vortex action. C.P. 1114, Ministry of Technology, Aeronautical Research Council, London, 1970.

[8] Gullbrand J and Fuchs L. A comparison of subgrid scale models for large eddy simulations of a co-annular swirling jet. Submitted for publication, 1999.

[9] Jeong J and Hussain F. On the identification of a vortex. *Journal of Fluid Mechanics*, Vol. 285, pp 69–94, 1995.

[10] Karlsson A and Fuchs L. Time evolution of the vortex between an air inlet and the ground. *Proc AIAA 38th Aerospace Science Meeting & Exhibit*, No 2000-0990, 2000.

[11] Liu W, Greitzer E. M, and Tan C. S. Surface static pressure in an inlet vortex flow field. *Journal of Engineering for Gas Turbines and Power*, Vol. 107, pp 387–393, april 1985.

[12] Motycka D. L and Walter W. A. An experimental investigation of ground vortex formation during reverse engine operation. *Proc AIAA/SAE 11th Propulsion Conference*, No 75-1322, Sep. 29-Oct. 1 1975.

[13] Motycka D. L, Walter W. A, and Muller G. L. An analytical and experimental study of inlet ground vortices. *Proc AIAA/SAE 9th Propulsion Conference*, No 73-1313, Nov. 5-7 1973.

[14] Nakayama A and Jones J. R. Vortex formation in inlet flow near a wall. *Proc AIAA 34th Aerospace Science Meeting & Exhibition*, No 96-0803, Jan. 15-18 1996.

[15] Nakayama A and Jones J. R. Correlation for formation of inlet vortex. *AIAA Journal*, Vol. 37, No 4, pp 508–510, 1999.

[16] Olsson M and Fuchs L. Large eddy simulation of the proximal region of a spatially developing circular jet. *Physics of Fluids*, Vol. 8, No 8, pp 2125–2137, 1996.

[17] Rodert L. A and Garrett F. B. Ingestion of foreign objects into turbine engines by vortices. NACA TN 3330, 1955.

[18] Shin H. W, Cheng W. K, Greitzer E. M, and Tan C. S. Inlet vortex formation due to ambient vorticity intensification. *AIAA Journal*, Vol. 24, No 4, pp 687–689, 1986.

[19] Shin H. W, Greitzer E. M, Cheng W. K, Tan C. S, and Shippee C. L. Circulation measurements and vorticity structure in an inlet-vortex flow field. *Journal of Fluid Mechanics*, Vol. 162, pp 463–487, 1986.